
Article:
Pastore, Alessandro (2020) Bootstrap analysis of the correlations between neutron skin thickness and the slope of symmetry energy. International journal of modern physics e-Nuclear physics. ISSN: 0218-3013

https://doi.org/10.1142/S0218301320500548

Received Day Month Year
Revised Day Month Year

Bootstrap analysis of the correlations between neutron skin thickness and the slope of symmetry energy

A. Pastore

Department of Physics, University of York, Heslington, York, Y010 5DD, UK

This work illustrates the use of bootstrap methods to quantify the statistical uncertainties on the correlation coefficients between the slope of the symmetry energy and the neutron skin thickness in heavy nuclei. By using several energy density functionals, I discuss the density dependence of such a correlation and its evolution with isospin asymmetry. In particular, I observe that the correlation between the slope of the symmetry energy and the neutron skin is present not only at saturation density, but over a much larger density range.

Keywords: nuclear matter, nuclear-structure models, bootstrap

PACS numbers:21.65.Mn 21.60.Jz nuclear-structure models

1. Introduction

The equation of state (EOS) of dense nuclear matter is the key ingredient to study the properties of massive astrophysical objects as neutron stars .[1] Several studies have shown that there is a strong correlation between properties of the EOS in infinite nuclear matter (INM) and various features of a neutron star (NS), such as the density, pressure, radii, maximum mass, cooling rate, and the crust-core transition.[2–15] Although properties of INM can not be measured directly, it is anyhow possible to relate some of them to observables of atomic nuclei: for example, information on nuclear incompressibility can be inferred by studying the behaviour of giant monopole resonances.[16,17]

In recent years, a series of articles on the possible correlation between the slope of the symmetry energy L_0[18] and the neutron skin thickness, Δr_{np}, in heavy nuclei has attracted a lot of attention:[19–22] thanks to this strong correlation, by performing accurate measurements of neutron skins thickness[23] it would be possible to put strong constraint on the resulting value of L_0 for a given nuclear model.

All these analysis are based on the use of a simple statistical estimator, the Pearson coefficients[24]

$$r = \frac{cov(X,Y)}{\sigma_X \sigma_Y} \ . \tag{1}$$

$cov(X,Y)$ is the covariance of two data-sets X, Y having variance σ_X^2, σ_Y^2 respectively. The coefficient r can take any value in the range $[-1,1]$. When $r \approx +1(-1)$,

one says that the two data-sets are correlated (anti-correlated) and, if $r \approx 0$, one says that the two data-sets are not correlated. It is worth noting that the results obtained with Eq.1 could be sometimes misleading since the correlation could be driven artificially by few outliers in the data-set. For more details, I refer to Ref. 25. To prevent such a problem, in Ref. 26 a more rigorous hypothesis testing has been illustrated. To this purpose is thus necessary to evaluate both the Pearson coefficient and its error bars. The latter should not be derived under the approximation of normality of the underlying distribution of the estimator via Fisher transformation[27] because this hypothesis breaks down if some outliers are present. See discussion in Ref. 26

To avoid such a problem, I illustrate a different statical approach based on non parametric bootstrap (NPB). NPB has been firstly introduced by Efron in 1979[28] and it relies on a very simple idea: given a data-set and a particular estimator (as for example the correlation coefficient in Eq.1); one builds new series of data-sets by resampling the original one. By applying the same estimators to the resulting data-sets, one gets the *empirical* distribution of the estimator. The hypothesis done by Efron is that such empirical distribution follows closely the *true* one. Having then access to the distribution of the estimator, it is possible to assess the error bars without postulating the type of the distribution as done using Fisher transformation. NPB is nowadays a common methodology used in several domain of science and a vast literature on the topic is available.[29–33]

The aim of the present article is to apply the NPB for a systematic assessment of the correlation between L_0 and Δr_{np} and in particular to evaluate how such a correlation evolves in function of other important quantities as the density of the nuclear medium and isospin asymmetry.

The article is organised as follows: in Sec.2 I introduce the models used to extract the information on neutron skin thickness, while I give a short introduction to NPB in Sec. 3. The results of my analysis are presented in Sec.4 for the ^{208}Pb case and extended in Sec.5 to other isotopic chains. In Sec.6, I briefly discuss the correlation with the symmetry energy and the role of the selected data-set. In Sec.7, I present my conclusions.

2. Neutron skin

Neutron skin thickness is defined as the difference between the radial extension of the neutron density against the proton one. This quantity has been very difficult to access experimentally and only recently thank to new pion-scattering methods,[23] it is now possible to measure it with very high accuracy.

From the theoretical point of view, the neutron skin thickness is usually extracted using a two-parameter Fermi function (2pF). The matter density of neutrons and protons is parametrised as

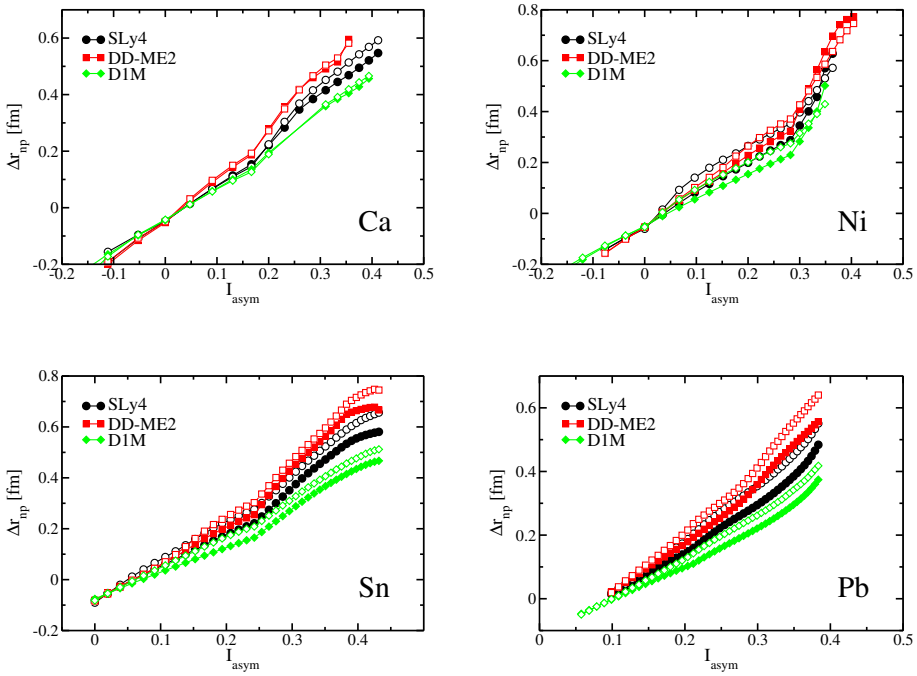

Fig. 1. (Colors online) Evolution of neutron skin as a function of isospin asymmetry $I_{asym} = \frac{N-Z}{N+Z}$ in different isotopic chains and different functionals. Filled symbols refer to the 2pF while open ones refer to Helm model calculations. See text for details.

$$\rho_q(r) = \frac{\rho_{0q}}{1 + \exp[(r - C_q)/a_q]} \ . \tag{2}$$

where $q = n, p$ is the isospin index that stands for neutron (n) and proton (p); ρ_{0q}, C_q, a_q are adjustable parameters. For a more detailed discussion I refer to Ref. 20 .

Although the matter densities can be extracted using several many-body methods, the tool of choice to describe the systematic behaviour of nuclei along the whole nuclear chart is the nuclear energy density functional (NEDF) theory.[34] In the present article, I will use a variety of functionals both non-relativistic as Skyrme[35] and Gogny[36] and relativistic[37] adjusted using various optimisation procedures.[38] By performing Hartree-Fock-Bogoliubov (HFB)[39] calculations using various functionals, I obtain the fully self-consistent matter densities and then fit the parameters of the 2pF to extract the resulting neutron skins.

In Ref 40, a different approach based on Helm model was proposed to extract neutron skin thicknesses. The main advantage of the Helm model is to obtain more

robust results that are independent on shell fluctuations in nuclear matter interior.[41] See Appendix A for details.

Apart from the very specific case of halo-nuclei,[42,43] there is no *a priori* reason to select 2pF over Helm model to extract the neutron skin thickness, as a consequence I will use both in my analysis.

In Fig.1, I show a systematic comparison of the neutron skin as a function of isospin asymmetry $I_{asym} = \frac{N-Z}{N+Z}$ calculated using different functionals: the zero-range Skyrme SLy4,[44] the finite-range Gogny D1M interaction[45] and the relativistic Lagrangian DD-ME2.[46] It is worth noting that for the D1M and DD-ME2 model, the pairing interaction is fixed and derived from a complete fitting procedure. The SLy4 functional, being fitted on double-magic nuclei only, leaves some freedom in adjusting the strength of the pairing interaction. In the present article I used the finite range interaction expressed in its separable form[47] adjusted to reproduce the pairing gaps of the Gogny D1S interaction in infinite nuclear matter.[48] I have checked, in Sn isotopes, that modifying the pairing interaction so that the pairing gap in ^{120}Sn varies between 1 to 2 MeV leads to a total change in the neutron skin of less than 3%. The role of pairing may be more important when approaching the drip-line, but in the present article I will study mainly very well bound nuclei and thus a very detailed analysis of pairing correlation is not necessary.

From Fig.1, I observe that 2pF and Helm model are very close to each other when $I_{asym} \approx 0$ and they start to deviate remarkably when $I_{asym} > 0.15$. In general, both methods provide similar trends, roughly independently on the selected functional, apart from the ending regions of each isotopic chains. It is important to observe that the difference between the skins extracted via 2pF and Helm model is not a simple constant shift, but one can clearly observe an isotopic dependence. It is thus important to keep both models for the following analysis.

3. Non-parametric bootstrap

Non-parametric bootstrap is a statistical method used to evaluate the bias of some particular estimators[28] . NPB is based on the simple assumption that any experimental data-set contains informations about its parent distribution thus, if the data-set is sufficiently large, one can simply replace the original parent distribution via the *empirical* one obtained from the sample. The latter is then approximated via Monte Carlo methods by performing resampling of the original data-set.

Following Ref 26, one assumes to have a data-set formed by n independent quantities $X = (x_1, x_2, \ldots, x_n)$ and a real-valued estimator of the parameter $\hat{\theta}$. The origin of the data is not specified and thus it could be derived either from a real experiment or from a simulation. The case of correlated data has been discussed in Refs 49, 50. From X, one re-samples the data creating a series of new data-sets called X^*. It is then possible to apply the estimator to this new set $\hat{\theta}^*$ and thus obtain its *empirical* distribution. Once one has such a distribution is then possible to extract informations concerning error bars.

It is important to notice that during the re-sampling of the original data-set, repetitions are allowed. For a data-set of size n, one can evaluate the number of possible combinations as

$$\binom{2n-1}{n} = \frac{(2n-1)!}{n!(n-1)!} \,. \tag{3}$$

Although there is no clear consensus in the literature on what would be the optimal value for n. It is clear that a too small value of n will give rise to a very limited amount of combinations and as such little information will be extracted from the method. It is worth mentioning, that NPB introduces an additional bias σ_B to the estimator that scales as $\frac{1}{N_B}$ where N_B is the number of Bootstrap samples generated. By taking $N_B \approx 3 \cdot 10^4$, as done here, the bias is then negligible. One can thus impose as a *safe* condition that the number of available combinations should be much larger than N_B. As a consequence a value of n larger than 10 will be enough. See Refs. 51, 52 for more details.

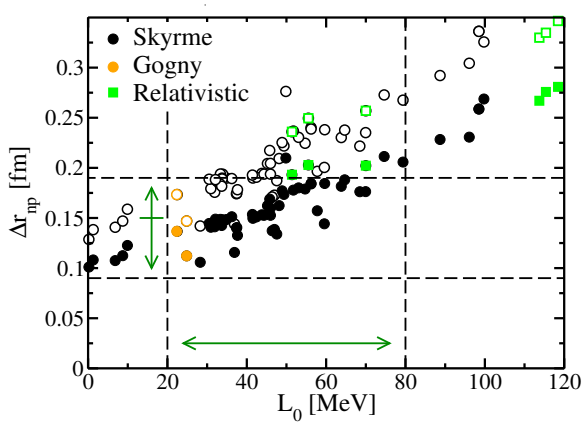

Fig. 2. (Colors online) Neutron skin thickness in ^{208}Pb as a function of L_0 for various models as given in Tab 1. Filled symbols refer to the 2pF while empty ones refer to Helm model calculations. See text for details

4. Results for ^{208}Pb

In this section, I study the correlation between slope of the symmetry energy at saturation density and Δr_{np} in ^{208}Pb. The interest in this nucleus is also related to the important effort done by the experimental community to improve the accuracy of the measurements of Δr_{np}.[23,53,54]

To extract Δr_{np}, I performed various Hartree-Fock (HF) calculations using selected functionals. In particular I considered 58 Skyrme functionals, 2 Gogny inter-

actions and 6 Lagrangians. In Tab. 1, I report the complete data set as well as the main infinite nuclear matter properties around saturation density ρ_0. The choice of the data set has been data to cover as much as possible the different families of functionals: the selected Skyrme functional include explicit 3-body terms,[55] higher order gradients[56] and additional density-dependent terms.[57,58] The Lagrangian used in this work contains a variety of model: density dependent,[46] point-coupling[59] and non linear density-independent models.[60] For a quick overview and comparison among the different models employed here, I refer the reader to Ref. 18 for Skyrme models and Ref. 60 for relativistic ones.

The slope of the symmetry energy is defined as the first derivative of the symmetry energy $J(\rho)$ evaluated at saturation density, $J_0 = J(\rho_0)$,

$$L_0 = 3\rho_0 \left.\frac{\partial J(\rho)}{\partial \rho}\right|_{\rho=\rho_0} \tag{4}$$

The typical range of variation of L_0 is quite large [18,60] with an interval spanning $L_0 \in [-500, 250]$ MeV. Clearly such a range of variation is probably too large especially when comparing with results extracted from *ab-initio* methods where one finds a value of $L_0 \approx 60$ MeV.[7] As a consequence, it is possible to use such an information to define a more reasonable interval of variation for L_0. In the present article, I selected functionals having an L_0 in the window $L_0 \in [0, 120]$. This choice is arbitrary, but it is compatible with the vast majority of current available constraints on this quantity (including error bars) coming from terrestrial or astrophysical measurements.[61]

By mean of a parabolic expansion,[62,63] one can write the EOS of asymmetric nuclear matter[64] as $\frac{E(\rho, I_{asym})}{A} = \frac{E(\rho)}{A} + \frac{E_{sym}(\rho)}{A} I_{asym}$, where $\frac{E(\rho)}{A}$ is the EOS of symmetric nuclear matter. The last term of this expression is usually written as a Taylor expansion around saturation density [65]

$$\frac{E_{sym}(\rho)}{A} \approx J_0 + L_0 \left(\frac{\rho - \rho_0}{\rho_0}\right) + \dots \tag{5}$$

By accurately constraining the value of J_0 and L_0 is thus possible to have a better understanding of the properties of the EOS in asymmetric matter around saturation. I refer to Ref. 66 to discuss the extra derivative terms appearing in Eq.5 and not reported here for simplicity.

4.1. *Bootstrap analysis*

Having introduced the basic idea of bootstrap and the data-set used for the analysis, I now perform the statistical analysis. In the two panels of Fig.2, I represent the results of the HF calculations using 66 values obtained with the chosen data-set: on the x-axis I report the values of the slope of the symmetry energy L_0 extracted

at saturation density and on the y-axis the neutron skin thickness defined either using the simple 2pF (filled symbols) and Helm model (empty symbols).

On the vertical axis, I have reported the most recent experimental value from Ref. 23 with its confidence interval. On horizontal axis, I have reported the acceptable value for L_0 as given in Ref. 18. In this case such an interval is not based on a direct measurements thus it has not the same statistical meaning of the confidence interval of the experimental measurement on the y-axis, but it can be viewed in a Bayesian approach as a prior knowledge acquired during several previous studies.[61]

By a simple visual inspection of Fig.2, one observes that all points lie on a line, independently on the way one extracts Δr_{np} (2pF or Helm). To quantify such a relation, I calculate the Pearson coefficient for the two models.[67] The result is $r = 0.94$ for the 2pF and $r = 0.93$ for the Helm model. The number alone has no meaning, since to determine if there is or not a correlation one has to make an hypothesis testing in a statistical sense.[24] To this purpose it is crucial to determine the confidence interval of such an estimator.

I apply NPB to the two data-sets following the procedure described in Sec.3. By performing $N_B = 3 \times 10^4$ Monte-Carlo iterations on the two data-sets, I obtain the distribution shown in Fig.3. Since Helm and 2pF results turn out to be quite similar, I report in the figure only the 2pF ones. The vertical lines indicate the 95% confidence interval. I obtained

$$\begin{aligned} \bar{r} &= 0.94^{+0.04}_{-0.04} \quad \text{2pF} \\ \bar{r} &= 0.93^{+0.04}_{-0.04} \quad \text{Helm} \end{aligned} \tag{6}$$

It is worth observing that the random re-sampling of the original data-set produces new sets of data where some of the points are either omitted or repeated. This is an excellent test to check the robustness of the selected data-set against possible outliers that may artificially drive the correlation. I refer to Ref. 26 for a specific example.

On the same figure, I also illustrate the distribution of the Spearman estimator.[68] The latter is a non-parametric measure of rank correlation. It assesses how well the relationship between two variables can be described using a monotonic function. Using different statistical tests is important since a given estimator can be fooled by a particular structure of the data-set. I apply the same NPB to this new test. The average values of Spearman coefficient $\bar{\rho}$ are

$$\begin{aligned} \bar{\rho} &= 0.90^{+0.05}_{-0.07} \quad \text{2pF} \\ \bar{\rho} &= 0.90^{+0.07}_{-0.07} \quad \text{Helm} \end{aligned} \tag{7}$$

In both cases, *i.e.* using $\bar{r}$ or $\bar{\rho}$, and for both 2pF and Helm model, it is possible to safely reject the null-hypothesis of non-correlated data with an accuracy larger than 95%. I conclude that the data set I used is robust and the correlation I observe is not associated with the specific choice of the data-set.

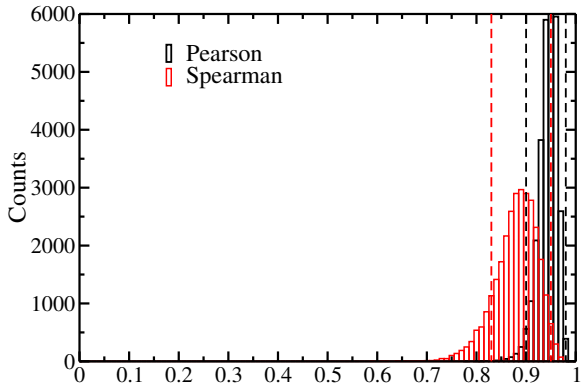

Fig. 3. (Colors online) Distribution of the correlation coefficients of the bootstrap data set for the 2pF model using Pearson and Spearman correlation tests in ^{208}Pb. Vertical lines indicate the interval containing 95% of the counts. See text for details.

These results simply confirm the findings in Ref. 19, but for a different group of functionals. This means that the observed correlation does not depend on the specific choice of the functionals used to form the data-set.

At this stage of the analysis it is also important to observe that for a given functional the resulting value of the skin strongly depends on the adopted model (Helm or 2pF) used to calculate Δr_{np}, as a consequence the value of L_0 constrained using possible experimental values will be model dependent. Such an additional source of uncertainty should then be properly taken into account in future analysis.

4.2. *Density dependence*

In the previous section, I have studied the correlation between L_0 and the neutron skin in ^{208}Pb. The correlation is very robust against the particular choice of the data-set, *i.e.* the choice of the NEDF used to perform the study and it is also robust in respect to the particular choice of the method used to extract Δr_{np} (2pF or Helm) and statistical estimator (Pearson or Spearman).

Since the nuclear density within a nucleus is not a constant, but it exhibits a strong position dependence, it is thus worth considering how the neutron skin of ^{208}Pb correlates, eventually, to the slope of the symmetry energy calculated at various densities. For completeness, I recall that $L(\rho)$ is calculated as

$$L(\rho) = 3\rho \frac{\partial J(\rho)}{\partial \rho} \quad , \tag{8}$$

where $J(\rho)$ is the symmetry energy. In Fig.4, I show the evolution of $L(\rho)$ as a function the density of the infinite medium for a subset of the functionals used in the current work. A very striking feature of Fig.4, is that each functional shows a

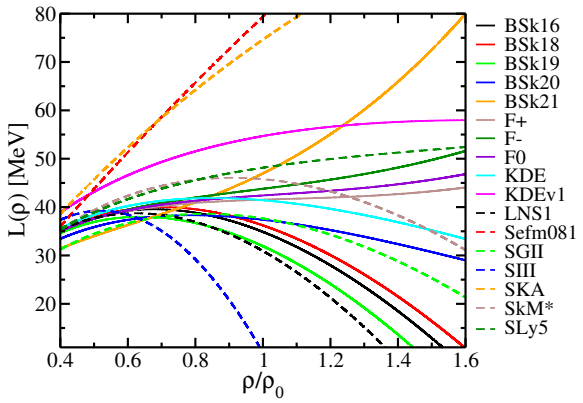

Fig. 4. (Colors online) Density dependence of the slope of the symmetry energy for a set of Skyrme functionals.

peculiar density dependence: for some functionals going from low to high density, $L(\rho)$ increases and for other functionals it decreases. In general one observes that in the low density region the spread is smaller than the one observed in high density, but the strong functional dependence is evident. This is not surprising since the explicitly density dependence of $L(\rho)$ is not typically constrained during fitting procedures as a consequence one observes such a large variance.

In Fig.5 (left panel), I show the scatter plot Δr_{np} extracted via 2pF model as a function of $L(\rho)$ for different values of the density of the infinite medium. One observes a striking *by eye* linear correlation between Δr_{np} and L at various density values. A similar results has been obtained using the Helm model and thus not reported in the figure.

To be more quantitative, in the right panel of Fig.5, I show the evolution of the Pearson coefficient for the different values of the density including the error bars corresponding to 95% confidence level as extracted via NPB methods. I actually observe a very strong correlation, *i.e.* $r > 0.9$, with reasonably small error bars on a large density interval $\rho \in [0.5\rho_{sat}, \rho_{sat}]$. On the same figure I also report the Spearman test $\bar{\rho}$ with very similar outcome. I actually observe that the maximum of the correlation between Δr_{np} and L takes place at $\rho/\rho_{sat} \approx 0.6 - 0.7$ where both tests give a very high value of correlation. Similar conclusions apply when using the Helm model to extract Δr_{np}. A similar conclusion was also obtained in Refs.[69,70] but using different methodologies.

At very low density, an anti-correlation seems to appear, but the error bars are so large that it is not possible to reject with enough accuracy the null hypothesis of non-correlation.

Given the behaviour of $L(\rho)$ shown in Fig.4 and the outcomes of Fig.5, I conclude that there is a persistent correlation between L and Δr_{np} in ^{208}Pb, but the exact values of density of infinite nuclear matter at which one should calculate L is not

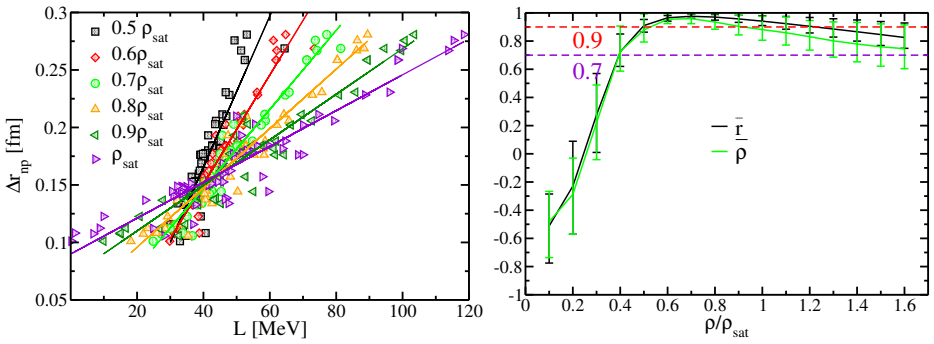

Fig. 5. (Colors online) Left panel: neutron skin thickness in ^{208}Pb as a function of $L(\rho)$ for dataset defined in Tab.1 at six distinct values of the density, solid lines are obtained with a linear regression simply to guide the eye. Right panel: evolution of Pearson coefficient $\bar{r}$ and Spearman coefficient $\bar{\rho}$ as a function of the density at which L is calculated according to Eq.8 for ^{208}Pb. See text for details.

clearly determined.

5. Isospin dependence

5.1. *Doubly-magic nuclei*

The previous analysis on ^{208}Pb points in the direction of strong correlation between neutron skin and slope of symmetry energy over a quite large density interval and different models. I repeat the analysis for other relevant doubly-magic nuclei as ^{40}Ca, ^{48}Ca, ^{56}Ni and ^{132}Sn.

In Fig.6, I report the results of the neutron skin extracted via 2pF and Helm model for these four doubly-magic nuclei. I observe that for ^{40}Ca and ^{56}Ni the are scattered and no clear trend is observed. In this case, both the Pearson and Spearman coefficients are very low and taking into account the error bars extracted via NPB I can affirm they are compatible with zero for any density at which $L(\rho)$ may be calculate. As discussed in Ref. 25, in N=Z nuclei the strong correlation disappears. This means that the possible proton skin is essentially governed by other effects as Coulomb interaction and very little related to the slope of the symmetry energy.

In the other two nuclei,*i.e.* ^{48}Ca and ^{132}Sn , the data nicely align although the slope of the intercept has a strong isospin dependence. For ^{48}Ca, I get $\bar{r} = 0.88^{+0.05}_{-0.06}$ using 2pF model at saturation, while for ^{132}Sn I obtain $\bar{r} = 0.94^{+0.03}_{-0.04}$. It is interesting to observe the evolution of such a correlation as a function of the density at which $L(\rho)$ is calculated. The results are presented in Fig.7 for both Pearson and Spearman coefficients with error bar as extracted via NPB method. For sake of simplicity I report only the results obtained with the 2pF model, but the one obtained with Helm model give very similar results.

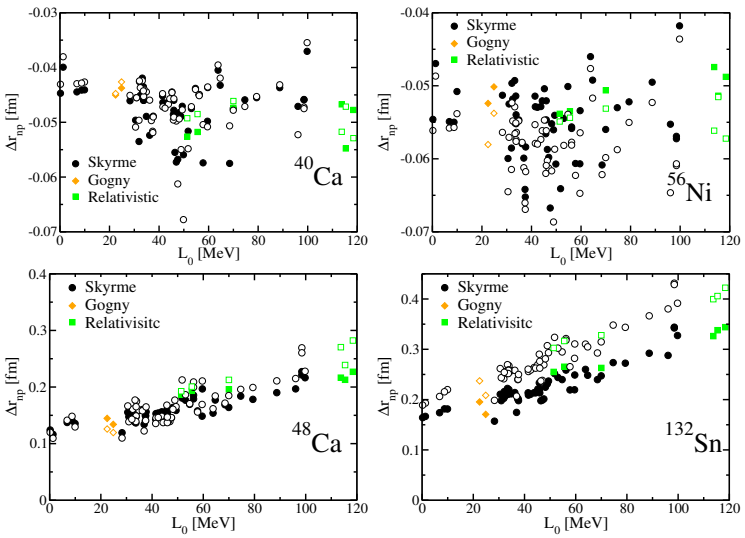

Fig. 6. (Colors online) Neutron skin extracted via 2pF (full symbols) and via Helm model (open symbols) as a function of the slope of the symmetry energy for different functionals and different nuclei. See text for details.

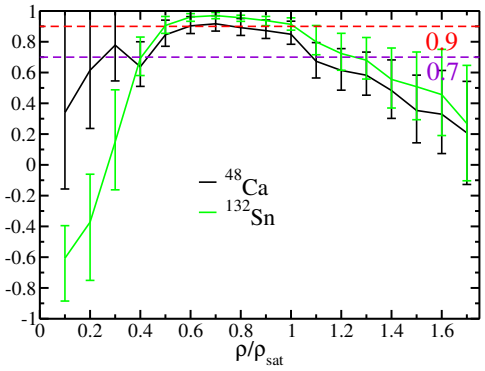

Fig. 7. (Colors online)Evolution of Pearson coefficient as a function of the density for ^{48}Ca and ^{132}Sn. See text for details.

I observe that, in a very similar way as shown in Fig.5, the correlations between $L(\rho)$ and Δr_{np} is quite robust and it extends over a wide range of densities, $\rho \in [0.5\rho_{sat}, \rho_{sat}]$

5.2. *Isotopic chains*

It is now interesting to focus on the possible isospin dependence of the $L_0, \Delta r_{np}$ correlation by investigating its evolution along some isotopic chains. According

to Ref. 71, it is possible to write a simple linear relation between L_0 and Δr_{np} via a droplet model. In this way, one observes a clear linear dependence on the neutron/proton asymmetry. This dependence has motivated the linear fit of Fig.2 done in Ref. 19 of various neutron skin thickness values obtained experimentally. In this section, I will investigate the validity of such an approximation.

In the left panel of Fig.8, I show how the neutron skin for selected tin isotopes correlates to the neutron skin calculated using 2pF model in ^{208}Pb. Although the alignment of the dots can be observe by naked eye, I have calculated using NPB the correlation coefficients of these data-sets and in all cases I have found a Pearson coefficient close to 0.99 with errors less than 1%. This means that all these data are strongly correlated against each other. It is interesting to analyse the correlation between ^{128}Sn and ^{208}Pb: the isospin asymmetry is $I_{asym} \approx 0.21$ for both nuclei The data deviate from the diagonal line (dotted line on the figure), the data-set of ^{124}Sn aligns almost perfectly along the diagonal despite having an asymmetry of $I_{asym} \approx 0.19$.

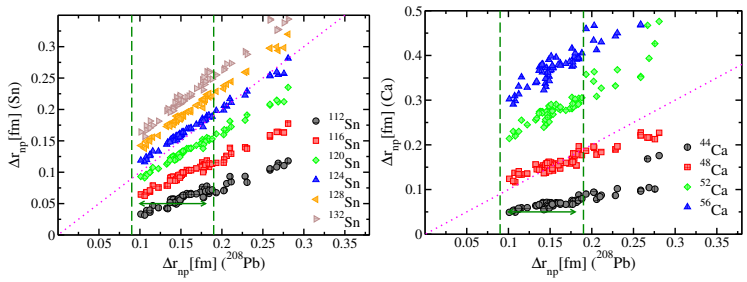

Fig. 8. (Colors online) Neutron skin in selected tin (left panel) and calcium (right panel) isotopes against neutron skin in ^{208}Pb. The dotted lines represents the diagonal and it is meant to guide the eye of the reader.See text for details

In the right panel Fig.8, I repeat the same analysis but for calcium isotopes. In this case the strong correlation at the diagonal point is with ^{48}Ca that has $I_{asym} \approx 0.16$. This figure illustrates that the linear dependence discussed in Ref. 19, it is an excellent first order approximation, but other effects may lead to deviations from linearity. A first corrective term that should be included into a possible linear fit, it is an explicit dependence on proton number as done in the simple droplet model. See Ref.72 for details.

In Fig.9, I show the evolution of the Pearson coefficient between Δr_{np} and L_0 as a function of the isospin asymmetry for four different isotopic chains: $^{36-70}$Ca, $^{52-90}$Ni, $^{100-176}Sn$ and $^{180-270}$Pb. It is worth noting that the length of the isotopic chains is not equal for all functionals, this means that for extremely neutron rich nuclei some functional do not predict the ground state to be bound and as such the datum is removed from the data-set.

The data are calculated using the 2pF to extract the neutron skin. I notice that results obtained with Helm model follow very closely and thus I do not show them on the figure, same conclusion applies for the Spearman estimator.

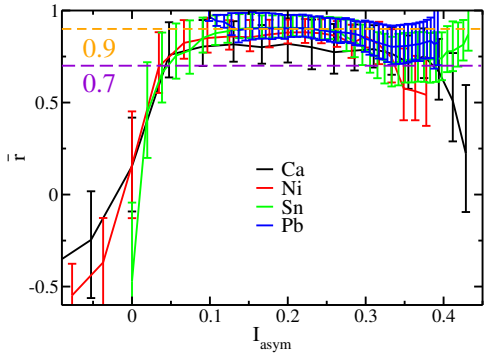

Fig. 9. (Colors online)Evolution of the Pearson correlation $\bar{r}$ for various isotopic chains chains. The neutron skin has been extracted using 2pF model. See text for details.

I observe that apart from the very low asymmetries, the correlation between Δr_{np} and L_0 is very robust in all nuclei and it is almost independent of the adopted asymmetry and on the number of nucleons in the nucleus. This means that such a correlation does not originates from particular shell effects, but it correlates to the bulk properties of the functionals used for the calculations.

6. Symmetry energy correlation

Symmetry energy J_0 is another important quantity used to constrain functional parameters. In this section, I thus repeated the same analysis done before using NPB to assess the correlation between J_0 and Δr_{np}. In Fig.10, I show the neutron skins calculated using various functionals as a function of J_0. In this case, I observe that the data are quite scattered.

By considering only the 2pF model in ^{208}Pb I find a Pearson correlation coefficient of $\bar{r} = 0.80^{0.07}_{-0.08}$ also very close to the Spearman estimator. On the right panel of Fig.10 I show the evolution of such a correlation as a function of the density at which J is calculated exactly in the same way as I did for L. For simplicity, I only report the Pearson coefficient in ^{208}Pb and ^{132}Sn and 2pF results. The ones obtained using Helm model are also very similar. In this case, I observe that below $0.8\rho_{sat}$ there is no correlation (or at least I can not exclude uncorrelated data), while around saturation density and well above the system always exhibits a quite good correlations. From this figure, I observe that there is a strong correlation in the density range $[1.1\rho_{sat}, 1.6\rho_{sat}]$. If one wants to use these data to constrain J by measuring skins, a particular attention should be paid to this possible ambiguity.

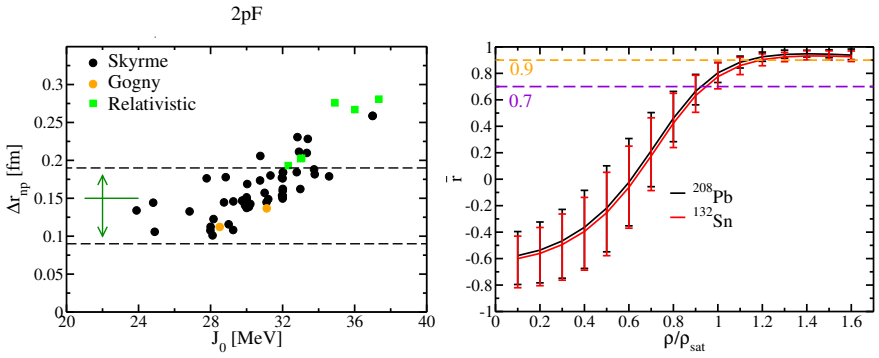

Fig. 10. (Colors online)Right panel: neutron skin thickness in ^{208}Pb calculated using 2pF model agains symmetry energy at saturation density. Left panel: evolution of the Pearson coefficient in ^{208}Pb and ^{132}Sn as a function of the density at which J is calculated.

It is very instructive to plot in Fig.11 the density dependence of J for a set of functionals used for the calculations. Similarly to Fig.4, there is no clear trend in the data: in some functionals J grows with the density and in other the opposite behaviour is observed. It is thus interesting to use a different data-set where other nuclear matter properties are better constrained. This analysis is presented in the following sub-section.

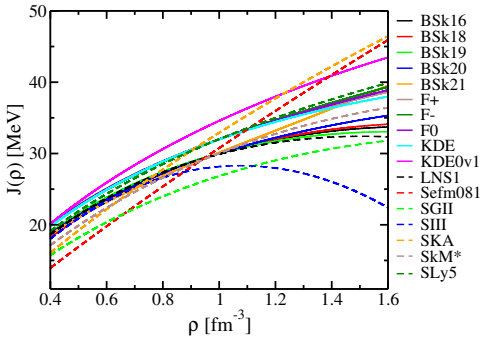

Fig. 11. (Colors online) Density dependence of the symmetry energy J for a set of Skyrme functionals.

6.1. *Different data-set*

In a recent article,[18] a selection of Skyrme models have been done by using a series of criteria derived from properties of nuclear matter around saturation density. Only 16 Skyrme functionals out of 240 satisfy these criteria (with a 5% tolerance).

I have reported them in Tab.2. By imposing several nuclear matter constraints, the resulting data-set shows a very little variation of the parameter L_0 at saturation density, despite the allowed range of variation being quite large $L_0 = 58 \pm 18$ MeV.[18] In Fig.12, I show the evolution of $J(\rho)$ and $L(\rho)$ as a function of the density for the selected functionals.

Compared to the results shown in Figs.4 and 11, one observes that the results are less scattered. This is particularly evident for $J(\rho)$, at least up to $1.6\rho_{sat}$. The slope of the symmetry energy still present some important variation at densities above saturation although such a variation is strongly reduced respected to the pool of functionals of Tab.1.

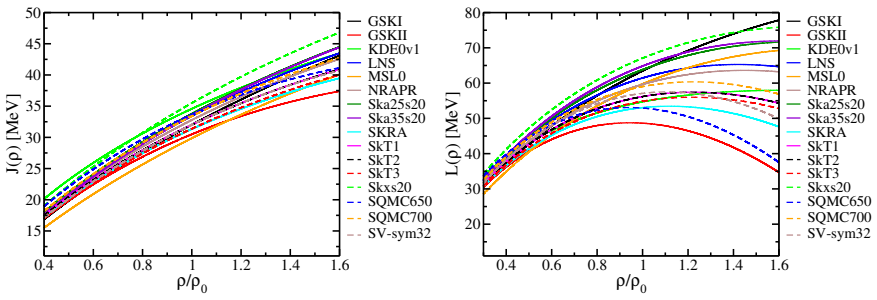

Fig. 12. (Colors online) Evolution of symmetry energy (left panel) and its slope (right) panel as a function of the density for the functionals given in Tab.2.

In Fig.13, I show the evolution of the neutron skin obtained with 2pF model in ^{208}Pb as a function of L_0 (top panel) and J_0 (lower panel). From the bootstrap analysis, I obtained a Pearson coefficient of $\bar{r} = 0.88^{0.09}_{-0.16}$ for the correlation with L_0 and $\bar{r} = 0.59^{0.38}_{-0.7}$ for the correlation with J_0. I observe that the correlation with L_0 is still present in this data-set while the one with J_0 is less certain, in particular one can not exclude the case of uncorrelated data given the large error bar on the estimator.

In Fig.14, I show the evolution of these two correlations as a function of the density of nuclear matter at which J and L have been calculated. It is interesting to note that the correlation with L is robust and I obtain the same conclusion already presented in Fig.5, with a maximum of the correlation around $\approx 0.5 - 0.6\rho_{sat}$. The correlation between the neutron skin and J is weak at low density and it starts to become more and more important at higher densities with a maximum at $1.6\rho_{sat}$. the result is in qualitative agreement with the one presented in Fig.10, although with some quantitative differences.

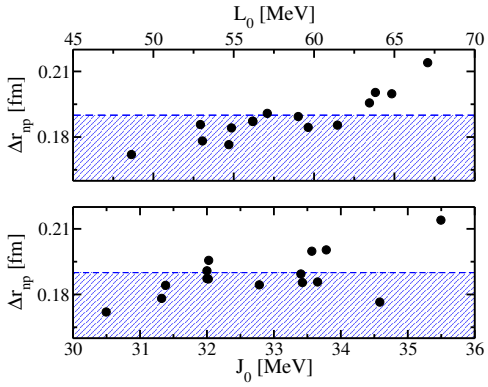

Fig. 13. (Colors online) Neutron skin thickness in ^{208}Pb as a function of L_0 (top panel) and J_0 (bottom panel) for the models given in Tab.2. The shaded area represents the region compatible with most recent measurements of neutron skin.[23]

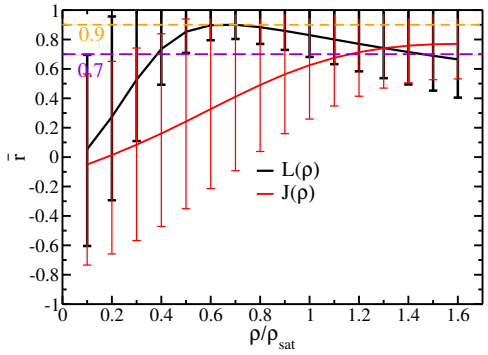

Fig. 14. (Colors online))Evolution of the Pearson correlation $\bar{r}$ for the correlation between Δr_{np} and the slope of the symmetry energy and between Δr_{np} and the symmetry energy. See text for details.

7. Conclusions

In the present article, I have used the non-parametric bootstrap method to the study of the correlation between the neutron skin thickness of heavy nuclei and the slope of the symmetry energy. This statistical method allows me to assess properties of the parent distribution thus making my conclusions more general and less dependent on the particular choice of the specific composition of the data-set employed in the calculations.

Although the numerical value of the neutron skin thickness changes when using Helm or 2pF to perform calculations, I showed that the correlation between Δr_{np} and L is very strong. To this purpose, I have checked that the result do not depend on the particular choice of the estimator (Pearson or Spearman).

A second important result is that there is no *a priori* indication to evaluate the correlation between Δr_{np} and L by arbitrary selecting the slope of the symmetry energy at saturation density: actually the analysis shows that the correlation is valid over a wide range of densities $[0.5-1]\rho_{sat}$. Since the variation of L with ρ is not model independent, one should pay particular attention before using such a correlation to constrain possible values of L_0 using information from Δr_{np}. Such a result confirms the findings of previous articles on the subject.[69,70]

I have also studied the possible correlation between the neutron skin thickness and the symmetry energy. In this case the correlation is weaker, but still present. More interesting the correlation seems to be more important at higher densities.

As a final comment, I stress that the results obtained here do not take into account the presence of error bars on the values of neutron skin extracted from HF(B) calculations.Since *all* functional come from a minimisation procedure a proper error propagation should be performed for each of the points used in the analysis. I refer to Ref 73 for a more detailed discussion.

Acknowledgments

I would like to thank X. Viñas for useful discussions and K. Bennaceur for providing me with Gogny results. This work has been supported by STFC Grant No. ST/P003885/1. Numerical calculations were performed using computational resources provided by the DiRAC Data Analytic system at the University of Cambridge, operated by the University of Cambridge High Performance Computing Service on behalf of the STFC DiRAC HPC Facility. This equipment was funded by BIS National E-infrastructure capital grant (ST/K001590/1), STFC capital grants ST/H008861/1 and ST/H00887X/1, and STFC DiRAC Operations grant ST/K00333X/1.

Appendix A. Helm model

The Helm model has been introduced in Ref. 40 to study properties of nuclear radii. The neutron skin is defined in this model as

$$\Delta R^H_{np} = \sqrt{\frac{5}{3}}\left(R^{(H)}_n - R^{(H)}_p\right) , \tag{A.1}$$

where $R^{(H)}_q$ is defined as

$$R^{(H)}_q = \sqrt{\frac{3}{5}(R^2_{0q} + 5\sigma^2_q)}. \tag{A.2}$$

The parameters R_{0q}, σ_q with $q = n, p$ are obtained by using the following equations

$$R_{0q} = 4.49341/q_{1q} \tag{A.3}$$

$$\sigma_q^2 = \frac{2}{q_{m,q}^2} \ln \frac{3R_{0q}^2 j_1(q_{m,q}R_{0q})}{R_{0q}q_{m,q}F(q_{m,q})} \ . \tag{A.4}$$

q_{1q} and $q_{m,q}$ represent the first zero and the first maximum of the form factor of the matter density defined as[42]

$$F_q(k) = 4\pi \int dr j_0(kr)\rho_q(r)r^2 \ . \tag{A.5}$$

j_l is the spherical Bessel function of order l.

Appendix B. Data set

In Tabs.1 and 2, I provide the detailed list of the functionals used in the present article together with some basic properties of infinite nuclear matter as saturation density, symmetry energy and its slope. These quantities have been calculated using the formalism presented in Refs 18, 60.

References

1. M. Baldo, *Nuclear methods and the nuclear equation of state*. World Scientific, 1999.
2. N. K. Glendenning, "Neutron-star masses as a constraint on the nuclear compression modulus," *Phys. Rev. Lett.*, vol. 57, pp. 1120–1123, Sep 1986.
3. C. J. Horowitz and J. Piekarewicz, "Neutron star structure and the neutron radius of ^{208}pb," *Phys. Rev. Lett.*, vol. 86, pp. 5647–5650, Jun 2001.
4. J. Piekarewicz, "Unmasking the nuclear matter equation of state," *Physical Review C*, vol. 69, no. 4, p. 041301, 2004.
5. J. M. Lattimer and M. Prakash, "Neutron star observations: Prognosis for equation of state constraints," *Physics reports*, vol. 442, no. 1, pp. 109–165, 2007.
6. J. Xu, L.-W. Chen, B.-A. Li, and H.-R. Ma, "Nuclear constraints on properties of neutron star crusts," *The Astrophysical Journal*, vol. 697, no. 2, p. 1549, 2009.
7. I. Vidaña, C. Providência, A. Polls, and A. Rios, "Density dependence of the nuclear symmetry energy: A microscopic perspective," *Phys. Rev. C*, vol. 80, p. 045806, Oct 2009.
8. C. Ducoin, J. Margueron, and C. Providência, "Nuclear symmetry energy and core-crust transition in neutron stars: A critical study," *EPL (Europhysics Letters)*, vol. 91, no. 3, p. 32001, 2010.
9. S. Gandolfi, J. Carlson, and S. Reddy, "Maximum mass and radius of neutron stars, and the nuclear symmetry energy," *Physical Review C*, vol. 85, no. 3, p. 032801, 2012.
10. F. J. Fattoyev and J. Piekarewicz, "Neutron skins and neutron stars," *Phys. Rev. C*, vol. 86, p. 015802, Jul 2012.
11. H. Sotani, K. Iida, and K. Oyamatsu, "Constraining the density dependence of the nuclear symmetry energy from an x-ray bursting neutron star," *Phys. Rev. C*, vol. 91, p. 015805, Jan 2015.
12. N. Alam, B. Agrawal, M. Fortin, H. Pais, C. Providência, A. R. Raduta, and A. Sulaksono, "Strong correlations of neutron star radii with the slopes of nuclear matter

	ρ_0 [fm^{-3}]	J_0 [MeV]	L_0 [MeV]		ρ_0 [fm^{-3}]	J_0 [MeV]	L_0 [MeV]
BSk16[74]	0.159	30.00	34.88	Ska25s20[18]	0.161	33.78	63.82
BSk18[75]	0.159	30.00	36.22	SkB [76]	0.155	23.89	47.56
BSk19[58]	0.160	30.00	31.9	SkM [77]	0.160	30.75	49.36
BSk20[58]	0.160	30.00	37.39	SLyMR1[55]	0.155	33.34	49.84
BSk21[58]	0.158	30.13	46.97	SkM* [78]	0.160	30.03	45.78
BSk22[79]	0.158	32.00	68.49	SKRA [80]	0.159	31.32	53.05
BSk23[79]	0.158	31.00	57.77	SkS1[81]	0.161	28.75	30.52
BSk24[79]	0.158	30.00	46.40	SkS3[81]	0.161	28.84	51.74
BSk25[79]	0.159	29.00	36.90	SkSC1[82]	0.161	28.11	0.21
BSk26 [79]	0.159	30.00	37.49	SkT[83]	0.148	24.90	28.27
F+[57]	0.162	32.00	41.54	SkT1[84]	0.161	32.02	56.19
F- [57]	0.162	32.00	43.79	SkT1a[18]	0.161	32.02	56.20
F0 [57]	0.162	32.00	42.41	SkT5[84]	0.164	37.00	98.50
KDE [85]	0.164	31.97	41.42	SkT5a[18]	0.164	37.00	98.50
KDE0v [85]	0.161	32.98	45.21	SkT9[84]	0.160	29.76	33.77
KDE0v1 [85]	0.165	34.58	54.69	SkT9a[18]	0.160	29.76	33.77
LNS1[86]	0.162	29.91	30.93	SKX[87]	0.155	31.11	33.23
MSk1[88]	0.157	30.00	33.92	SKXce[87]	0.155	30.21	33.67
MSk2[88]	0.157	30.00	33.35	SKXm[87]	0.159	31.20	32.09
MSk3[88]	0.158	27.99	6.83	SLy230a[44]	0.160	31.99	44.33
NRAPR [89]	0.161	32.78	59.63	SLy230b[44]	0.160	32.01	45.97
RATP[90]	0.160	29.26	32.43	SLy4[44]	0.160	32.00	45.96
Sefm074[18]	0.160	33.40	88.71	SLy5[44]	0.161	32.01	48.15
Sefm081[18]	0.161	30.76	79.38	SQMC750[91]	0.171	33.75	64.67
Sefm09[18]	0.161	27.78	69.95	SV[92]	0.155	32.82	96.07
Sefm1[18]	0.161	24.81	59.55	v100[93]	0.157	28.00	8.73
SGII [94]	0.158	26.83	37.66	D1M [45] (G)	0.164	28.50	24.85
SGOI [95]	0.168	45.20	99.76	D1S [36] (G)	0.163	31.12	22.46
SI [96]	0.155	29.25	1.29	DD-PC1[59] (R)	0.152	33.00	70.00
SIII [97]	0.145	28.16	9.91	DD-ME1[46](R)	0.152	33.06	55.53
SkA [76]	0.155	32.91	74.62	DD-ME2[46] (R)	0.152	32.31	51.39
SN2LO1[56]	0.162	31.96	48.89	NLSH[98] (R)	0.145	36.01	113.74
NL3[98] (R)	0.148	37.35	118.44	LHS[37] (R)	0.148	34.99	115.60

Table 1. Infinite matter properties of the data-set used in the current analysis. I indicate with (R) the relativistic models and with (G) the finite range one.

incompressibility and symmetry energy at saturation," *Physical Review C*, vol. 94, no. 5, p. 052801, 2016.

13. M. Fortin, C. Providência, A. R. Raduta, F. Gulminelli, J. L. Zdunik, P. Haensel, and M. Bejger, "Neutron star radii and crusts: Uncertainties and unified equations

	ρ_0 [fm^{-3}]	J_0 [MeV]	L_0 [MeV]		ρ_0 [fm^{-3}]	J_0 [MeV]	L_0 [MeV]
LNS[99]	0.175	33.43	61.45	MSL0[100]	0.160	29.87	59.77
Ska25s20[18]	0.161	33.78	63.82	Ska35s20[18]	0.158	33.56	64.83
SQMC650[91]	0.172	33.65	52.94	SKRA [80]	0.159	31.32	53.05
SQMC700[91]	0.170	33.40	59.01	SkT1[84]	0.161	32.02	56.19
SV-sym32[101]	0.159	32.00	57.09	SkT2[84]	0.161	32.00	56.18
GSKI[102]	0.159	32.02	63.48	SkT3[84]	0.161	31.38	54.86
GSkII[102]	0.159	30.50	48.63	Skxs20[103]	0.161	35.49	67.07
KDE0v1 [85]	0.165	34.58	54.69	NRAPR [89]	0.161	32.78	59.63

Table 2. Infinite matter properties of the Skyrme functionals selected in Ref.[18]

of state," *Phys. Rev. C*, vol. 94, p. 035804, Sep 2016.
14. M. Dutra, O. Lourenço, and D. P. Menezes, "Stellar properties and nuclear matter constraints," *Phys. Rev. C*, vol. 93, p. 025806, Feb 2016.
15. T. Malik, N. Alam, M. Fortin, C. Providência, B. Agrawal, T. Jha, B. Kumar, and S. Patra, "Gw170817: Constraining the nuclear matter equation of state from the neutron star tidal deformability," *Physical Review C*, vol. 98, no. 3, p. 035804, 2018.
16. J. Blaizot, D. Gogny, and B. Grammaticos, "Nuclear compressibility and monopole resonances," *Nuclear Physics A*, vol. 265, no. 2, pp. 315–336, 1976.
17. P. Veselỳ, J. Toivanen, B. Carlsson, J. Dobaczewski, N. Michel, and A. Pastore, "Giant monopole resonances and nuclear incompressibilities studied for the zero-range and separable pairing interactions," *Physical Review C*, vol. 86, no. 2, p. 024303, 2012.
18. M. Dutra, O. Lourenço, J. S. Sá Martins, A. Delfino, J. R. Stone, and P. D. Stevenson, "Skyrme interaction and nuclear matter constraints," *Phys. Rev. C*, vol. 85, p. 035201, Mar 2012.
19. M. Centelles, X. Roca-Maza, X. Viñas, and M. Warda, "Nuclear symmetry energy probed by neutron skin thickness of nuclei," *Phys. Rev. Lett.*, vol. 102, p. 122502, Mar 2009.
20. M. Warda, X. Viñas, X. Roca-Maza, and M. Centelles, "Analysis of bulk and surface contributions in the neutron skin of nuclei," *Phys. Rev. C*, vol. 81, p. 054309, May 2010.
21. X. Roca-Maza, M. Centelles, X. Viñas, and M. Warda, "Neutron skin of ^{208}Pb, nuclear symmetry energy, and the parity radius experiment," *Phys. Rev. Lett.*, vol. 106, p. 252501, Jun 2011.
22. X. Viñas, M. Centelles, X. Roca-Maza, and M. Warda, "Density dependence of the symmetry energy from neutron skin thickness in finite nuclei," *The European Physical Journal A*, vol. 50, no. 2, pp. 1–16, 2014.
23. C. Tarbert, D. Watts, D. Glazier, P. Aguar, J. Ahrens, J. Annand, H. Arends, R. Beck, V. Bekrenev, B. Boillat, *et al.*, "Neutron skin of pb 208 from coherent pion photoproduction," *Physical review letters*, vol. 112, no. 24, p. 242502, 2014.
24. R.J.Barlow, *A Guide to the Use of Statistical Methods in the Physical Sciences*. John Wiley, 1989.
25. D. Muir, A. Pastore, J. Dobaczewski, and C. Barton, "Bootstrap technique to study correlation between neutron skin thickness and the slope of symmetry energy in

atomic nuclei," *Acta Physica Polonica B*, vol. 49, no. 3, 2018.
26. A. Pastore, "An introduction to bootstrap for nuclear physics," *Journal of Physics G: Nuclear and Particle Physics*, vol. 46, no. 5, p. 052001, 2019.
27. D. M. Corey, W. P. Dunlap, and M. J. Burke, "Averaging correlations: Expected values and bias in combined pearson rs and fisher's z transformations," *The Journal of general psychology*, vol. 125, no. 3, pp. 245–261, 1998.
28. B. Efron, "Bootstrap methods, another look at the jackknife," *Annals of Statistics*, vol. 7, pp. 1–26, 1979.
29. B. Efron and R. Tibshirani, *An introduction to the bootstrap*. CRC press, 1994.
30. A. C. Davison and D. V. Hinkley, *Bootstrap methods and their application*, vol. 1. Cambridge university press, 1997.
31. B. F. Manly, *Randomization, bootstrap and Monte Carlo methods in biology*, vol. 70. CRC press, 2006.
32. M. R. Chernick, *Bootstrap methods: a guide for practitioners and researchers*, vol. 1. Wiley-Interscience, 2008.
33. M. R. Chernick, W. González-Manteiga, R. M. Crujeiras, and E. B. Barrios, "Bootstrap methods," in *International encyclopedia of statistical science*, pp. 169–174, Springer, 2011.
34. M. Bender, P.-H. Heenen, and P.-G. Reinhard, "Self-consistent mean-field models for nuclear structure," *Reviews of Modern Physics*, vol. 75, no. 1, p. 121, 2003.
35. T. Skyrme, "The effective nuclear potential," *Nuclear Physics*, vol. 9, no. 4, pp. 615–634, 1958.
36. J. Dechargé and D. Gogny, "Hartree-fock-bogolyubov calculations with the d 1 effective interaction on spherical nuclei," *Physical Review C*, vol. 21, no. 4, p. 1568, 1980.
37. P.-G. Reinhard, "The relativistic mean-field description of nuclei and nuclear dynamics," *Reports on Progress in Physics*, vol. 52, no. 4, p. 439, 1989.
38. M. Kortelainen, T. Lesinski, J. Moré, W. Nazarewicz, J. Sarich, N. Schunck, M. Stoitsov, and S. Wild, "Nuclear energy density optimization," *Physical Review C*, vol. 82, no. 2, p. 024313, 2010.
39. P.Ring and P.Schuck, *The Nuclear Many-Body Problem*. Springer-Verlag Berlin Heidelberg, 1980.
40. S. Mizutori, J. Dobaczewski, G. A. Lalazissis, W. Nazarewicz, and P.-G. Reinhard, "Nuclear skins and halos in the mean-field theory," *Phys. Rev. C*, vol. 61, p. 044326, Mar 2000.
41. P. Durgapal and D. Onley, "Charge and current distributions in the helm model," *Nuclear Physics A*, vol. 368, no. 3, pp. 429–437, 1981.
42. V. Rotival and T. Duguet, "New analysis method of the halo phenomenon in finite many-fermion systems: First applications to medium-mass atomic nuclei," *Physical Review C*, vol. 79, no. 5, p. 054308, 2009.
43. V. Rotival, K. Bennaceur, and T. Duguet, "Halo phenomenon in finite many-fermion systems: Atom-positron complexes and large-scale study of atomic nuclei," *Physical Review C*, vol. 79, no. 5, p. 054309, 2009.
44. E. Chabanat, P. Bonche, P. Haensel, J. Meyer, and R. Schaeffer, "A skyrme parametrization from subnuclear to neutron star densities," *Nuclear Physics A*, vol. 627, no. 4, pp. 710–746, 1997.
45. S. Goriely, S. Hilaire, M. Girod, and S. Péru, "First gogny-hartree-fock-bogoliubov nuclear mass model," *Physical review letters*, vol. 102, no. 24, p. 242501, 2009.
46. G. Lalazissis, T. Nikšić, D. Vretenar, and P. Ring, "New relativistic mean-field interaction with density-dependent meson-nucleon couplings," *Physical Review C*, vol. 71,

no. 2, p. 024312, 2005.
47. T. Duguet, "Bare vs effective pairing forces: A microscopic finite-range interaction for Hartree-Fock-Bogolyubov calculations in coordinate space," *Physical Review C*, vol. 69, p. 054317, 2004.
48. A. Pastore, J. Margueron, P. Schuck, and X. Viñas, "Pairing in exotic neutron-rich nuclei near the drip line and in the crust of neutron stars," *Physical Review C*, vol. 88, no. 3, p. 034314, 2013.
49. G. Bertsch and D. Bingham, "Estimating parameter uncertainty in binding-energy models by the frequency-domain bootstrap," *Physical review letters*, vol. 119, no. 25, p. 252501, 2017.
50. A. Pastore, D. Neill, H. Powell, K. Medler, and C. Barton, "Impact of statistical uncertainties on the composition of the outer crust of a neutron star," *Physical Review C*, vol. 101, no. 3, p. 035804, 2020.
51. E. Nieves, J.and Ruiz Arriola, "Error estimates for $\pi\pi$ scattering threshold parameters in chiral perturbation theory to two loops," *The European Physical Journal A*, vol. 8, pp. 377–384, Sep 2000.
52. R. N. Pérez, J. Amaro, and E. R. Arriola, "Bootstrapping the statistical uncertainties of nn scattering data," *Physics Letters B*, vol. 738, pp. 155–159, 2014.
53. R. Michaels, "The lead radius experiment prex," *Hyperfine Interactions*, vol. 201, no. 1-3, pp. 25–29, 2011.
54. C. J. Horowitz, K. S. Kumar, and R. Michaels, "Electroweak measurements of neutron densities in crex and prex at jlab, usa," *The European Physical Journal A*, vol. 50, no. 2, p. 48, 2014.
55. J. Sadoudi, M. Bender, K. Bennaceur, D. Davesne, R. Jodon, and T. Duguet, "Skyrme pseudo-potential-based edf parametrization for spuriousity-free mr edf calculations," *Physica Scripta*, vol. 2013, no. T154, p. 014013, 2013.
56. P. Becker, D. Davesne, J. Meyer, J. Navarro, and A. Pastore, "Solution of hartree-fock-bogoliubov equations and fitting procedure using the n2lo skyrme pseudopotential in spherical symmetry," *Physical Review C*, vol. 96, no. 4, p. 044330, 2017.
57. T. Lesinski, K. Bennaceur, T. Duguet, and J. Meyer, "Isovector splitting of nucleon effective masses, ab initio benchmarks and extended stability criteria for Skyrme energy functionals," *Physical Review C*, vol. 74, p. 044315, 2006.
58. S. Goriely, N. Chamel, and J. M. Pearson, "Further explorations of skyrme-hartree-fock-bogoliubov mass formulas. xii. stiffness and stability of neutron-star matter," *Phys. Rev. C*, vol. 82, p. 035804, Sep 2010.
59. T. Nikšić, D. Vretenar, and P. Ring, "Relativistic nuclear energy density functionals: Adjusting parameters to binding energies," *Physical Review C*, vol. 78, no. 3, p. 034318, 2008.
60. M. Dutra, O. Lourenço, S. Avancini, B. Carlson, A. Delfino, D. Menezes, C. Providência, S. Typel, and J. Stone, "Relativistic mean-field hadronic models under nuclear matter constraints," *Physical Review C*, vol. 90, no. 5, p. 055203, 2014.
61. W. G. Newton, J. Hooker, M. Gearheart, K. Murphy, D.-H. Wen, F. J. Fattoyev, and B.-A. Li, "Constraints on the symmetry energy from observational probes of the neutron star crust," *The European Physical Journal A*, vol. 50, no. 2, p. 41, 2014.
62. M. Lopez-Quelle, S. Marcos, R. Niembro, A. Bouyssy, and N. Van Giai, "Asymmetric nuclear matter in the relativistic approach," *Nuclear Physics A*, vol. 483, no. 3-4, pp. 479–492, 1988.
63. V. Baran, M. Colonna, V. Greco, and M. Di Toro, "Reaction dynamics with exotic nuclei," *Physics Reports*, vol. 410, no. 5-6, pp. 335–466, 2005.

64. B. Liu, V. Greco, V. Baran, M. Colonna, and M. Di Toro, "Asymmetric nuclear matter: The role of the isovector scalar channel," *Physical Review C*, vol. 65, no. 4, p. 045201, 2002.
65. B.-A. Li, L.-W. Chen, and C. M. Ko, "Recent progress and new challenges in isospin physics with heavy-ion reactions," *Physics Reports*, vol. 464, no. 4-6, pp. 113–281, 2008.
66. C. Gonzalez-Boquera, M. Centelles, X. Viñas, and A. Rios, "Higher-order symmetry energy and neutron star core-crust transition with gogny forces," *Physical Review C*, vol. 96, no. 6, p. 065806, 2017.
67. J. Hauke and T. Kossowski, "Comparison of values of pearson's and spearman's correlation coefficients on the same sets of data," *Quaestiones geographicae*, vol. 30, no. 2, p. 87, 2011.
68. S. Yue, P. Pilon, and G. Cavadias, "Power of the mann–kendall and spearman's rho tests for detecting monotonic trends in hydrological series," *Journal of hydrology*, vol. 259, no. 1, pp. 254–271, 2002.
69. E. Khan, J. Margueron, and I. Vidana, "Constraining the nuclear equation of state at subsaturation densities," *Physical review letters*, vol. 109, no. 9, p. 092501, 2012.
70. Z. Zhang and L.-W. Chen, "Constraining the symmetry energy at subsaturation densities using isotope binding energy difference and neutron skin thickness," *Physics Letters B*, vol. 726, no. 1-3, pp. 234–238, 2013.
71. M. Warda, X. Vinas, X. Roca-Maza, and M. Centelles, "Neutron skin thickness in the droplet model with surface width dependence: Indications of softness of the nuclear symmetry energy," *Physical Review C*, vol. 80, no. 2, p. 024316, 2009.
72. W. D. Myers and W. Swiatecki, "Average nuclear properties," *Annals Phys.*, vol. 55, p. 395, 1969.
73. T. Haverinen and M. Kortelainen, "Uncertainty propagation within the unedf models," *Journal of Physics G: Nuclear and Particle Physics*, vol. 44, no. 4, p. 044008, 2017.
74. N. Chamel, S. Goriely, and J. Pearson, "Further explorations of skyrme–hartree–fock–bogoliubov mass formulas. ix: Constraint of pairing force to 1s0 neutron-matter gap," *Nuclear Physics A*, vol. 812, no. 1-4, pp. 72–98, 2008.
75. N. Chamel and S. Goriely, "Spin and spin-isospin instabilities in asymmetric nuclear matter at zero and finite temperatures using Skyrme functionals," *Physical Review C*, vol. 82, p. 045804, Oct. 2010.
76. H. Köhler, "Skyrme force and the mass formula," *Nuclear Physics A*, vol. 258, no. 2, pp. 301–316, 1976.
77. H. Krivine, J. Treiner, and O. Bohigas, "Derivation of a fluid-dynamical lagrangian and electric giant resonances," *Nuclear Physics A*, vol. 336, no. 2, pp. 155–184, 1980.
78. J. Bartel, P. Quentin, M. Brack, C. Guet, and H.-B. Håkansson, "Towards a better parametrisation of skyrme-like effective forces: A critical study of the skm force," *Nuclear Physics A*, vol. 386, no. 1, pp. 79–100, 1982.
79. S. Goriely, N. Chamel, and J. Pearson, "Further explorations of skyrme-hartree-fock-bogoliubov mass formulas. xiii. the 2012 atomic mass evaluation and the symmetry coefficient," *Physical Review C*, vol. 88, no. 2, p. 024308, 2013.
80. M. Rashdan, "A skyrme parametrization based on nuclear matter bhf calculations," *Modern Physics Letters A*, vol. 15, no. 20, pp. 1287–1299, 2000.
81. J. Gómez, C. Prieto, and J. Navarro, "Improved skyrme forces for hartree-fock seniority calculations," *Nuclear Physics A*, vol. 549, no. 1, pp. 125–142, 1992.
82. M. Onsi, H. Przysiezniak, and J. Pearson, "Equation of state of homogeneous nuclear matter and the symmetry coefficient," *Physical Review C*, vol. 50, no. 1, p. 460, 1994.

83. C. Ko, H. Pauli, M. Brack, and G. Brown, "A microscopic, but not self-consistent approach to nuclear binding and deformation energies," *Nuclear Physics A*, vol. 236, no. 2, pp. 269–301, 1974.
84. F. Tondeur, M. Brack, M. Farine, and J. Pearson, "Static nuclear properties and the parametrisation of skyrme forces," *Nuclear Physics A*, vol. 420, no. 2, pp. 297–319, 1984.
85. B. Agrawal, S. Shlomo, and V. K. Au, "Determination of the parameters of a skyrme type effective interaction using the simulated annealing approach," *Physical Review C*, vol. 72, no. 1, p. 014310, 2005.
86. D. Gambacurta, L. Li, G. Colo, U. Lombardo, N. Van Giai, and W. Zuo, "Determination of local energy density functionals from brueckner-hartree-fock calculations," *Physical Review C*, vol. 84, no. 2, p. 024301, 2011.
87. B. A. Brown, "New skyrme interaction for normal and exotic nuclei," *Physical Review C*, vol. 58, no. 1, p. 220, 1998.
88. F. Tondeur, S. Goriely, J. Pearson, and M. Onsi, "Towards a hartree-fock mass formula," *Physical Review C*, vol. 62, no. 2, p. 024308, 2000.
89. A. W. Steiner, M. Prakash, J. M. Lattimer, and P. J. Ellis, "Isospin asymmetry in nuclei and neutron stars," *Physics reports*, vol. 411, no. 6, pp. 325–375, 2005.
90. M. Rayet, M. Arnould, G. Paulus, and F. Tondeur, "Nuclear forces and the properties of matter at high temperature and density," *Astronomy and Astrophysics*, vol. 116, pp. 183–187, 1982.
91. P. A. Guichon, H. H. Matevosyan, N. Sandulescu, and A. W. Thomas, "Physical origin of density dependent forces of skyrme type within the quark meson coupling model," *Nuclear Physics A*, vol. 772, no. 1-2, pp. 1–19, 2006.
92. M. Beiner, H. Flocard, N. Van Giai, and P. Quentin, "Nuclear ground-state properties and self-consistent calculations with the skyrme interaction:(i). spherical description," *Nuclear Physics A*, vol. 238, no. 1, pp. 29–69, 1975.
93. J. Pearson and S. Goriely, "Isovector effective mass in the skyrme-hartree-fock method," *Physical Review C*, vol. 64, no. 2, p. 027301, 2001.
94. N. Van Giai and H. Sagawa, "Spin-isospin and pairing properties of modified skyrme interactions," *Physics Letters B*, vol. 106, no. 5, pp. 379–382, 1981.
95. Q.-b. Shen, Y.-l. Han, H.-r. Guo, *et al.*, "Isospin dependent nucleon-nucleus optical potential with skyrme interactions," *Physical Review C*, vol. 80, no. 2, p. 024604, 2009.
96. D. Vautherin, "D. vautherin and dm brink, phys. rev. c 5, 626 (1972).," *Phys. Rev. C*, vol. 5, p. 626, 1972.
97. M. Giannoni and P. Quentin, "Mass parameters in the adiabatic time-dependent hartree-fock approximation. ii. results for the isoscalar quadrupole mode," *Physical Review C*, vol. 21, no. 5, p. 2076, 1980.
98. G. Lalazissis, J. König, and P. Ring, "New parametrization for the lagrangian density of relativistic mean field theory," *Physical Review C*, vol. 55, no. 1, p. 540, 1997.
99. L. G. Cao, U. Lombardo, C. W. Shen, and N. V. Giai, "From brueckner approach to skyrme-type energy density functional," *Phys. Rev. C*, vol. 73, p. 014313, Jan 2006.
100. S. Typel and B. A. Brown, "Neutron radii and the neutron equation of state in relativistic models," *Phys. Rev. C*, vol. 64, p. 027302, Jun 2001.
101. P. Klüpfel, P.-G. Reinhard, T. J. Bürvenich, and J. A. Maruhn, "Variations on a theme by skyrme: A systematic study of adjustments of model parameters," *Phys. Rev. C*, vol. 79, p. 034310, Mar 2009.
102. B. K. Agrawal, S. K. Dhiman, and R. Kumar, "Exploring the extended density-dependent skyrme effective forces for normal and isospin-rich nuclei to neutron

stars," *Phys. Rev. C*, vol. 73, p. 034319, Mar 2006.
103. B. A. Brown, G. Shen, G. C. Hillhouse, J. Meng, and A. Trzcińska, "Neutron skin deduced from antiprotonic atom data," *Phys. Rev. C*, vol. 76, p. 034305, Sep 2007.